JVI Journals.ASM.org

Ifit2 Deficiency Results in Uncontrolled Neurotropic Coronavirus Replication and Enhanced Encephalitis via Impaired Alpha/Beta Interferon Induction in Macrophages

Niranjan B. Butchi,[a]† David R. Hinton,[b] Stephen A. Stohlman,[a] Parul Kapil,[a] Volker Fensterl,[c] Ganes C. Sen,[c] Cornelia C. Bergmann[a]

Department of Neurosciences, Lerner Research Institute, The Cleveland Clinic Foundation, Cleveland, Ohio, USA[a]; Department of Pathology, Keck School of Medicine, University of Southern California, Los Angeles, California, USA[b]; Department of Molecular Genetics, Lerner Research Institute, The Cleveland Clinic Foundation, Cleveland, Ohio, USA[c]

Type I interferons (IFN-α/β) limit viral dissemination prior to the emergence of adaptive immune responses through the concerted action of interferon-stimulated genes (ISGs). Although IFN-α/β induction by coronaviruses is modest, it effectively limits viral spread within the central nervous system (CNS) and protects against mortality. The protective roles of specific ISGs against the mouse hepatitis virus (MHV) members of the coronaviruses are largely unknown. This study demonstrates a protective role of the ISG *Ifit2* in encephalitis induced by the dual hepato- and neurotropic MHV-A59. Contrasting the mild encephalitis and 100% survival of MHV-A59-infected wild-type (wt) mice, nearly 60% of infected *Ifit2*$^{-/-}$ mice exhibited severe encephalitis and succumbed between 6 and 8 days postinfection. Increased clinical disease in *Ifit2*$^{-/-}$ mice coincided with higher viral loads and enhanced viral spread throughout the CNS parenchyma. *Ifit2*$^{-/-}$ mice also expressed significantly reduced IFN-α/β and downstream ISG mRNAs *Ifit1*, *Isg15*, and *Pkr*, while expression of proinflammatory cytokines and chemokines was only modestly affected in the CNS. Impaired IFN-α/β induction in the absence of *Ifit2* was confirmed by *ex vivo* mRNA analysis of microglia and macrophages, the prominent cell types producing IFN-α/β following MHV CNS infection. Furthermore, both IFN-α/β mRNA and protein production were significantly reduced in MHV-infected *Ifit2*$^{-/-}$ relative to wt bone marrow-derived macrophages. Collectively, the data implicate Ifit2 as a positive regulator of IFN-α/β expression, rather than direct antiviral mediator, during MHV-induced encephalitis.

Type I interferons (IFN-α/β) provide a first line of defense against viral infections by limiting dissemination prior to the emergence of adaptive immune responses. Viral infection is sensed by endosomal Toll-like receptors (TLRs) or cytosolic retinoic acid-inducible gene I (RIG-I)-like receptors, which signal to activate NF-κB, IFN-regulatory factor 3 (IRF3), IRF7, and downstream transcription of cytokine and IFN-α/β genes (1, 2). IFN-α/β binding to its receptor induces JAK/STAT signaling and upregulation of hundreds of IFN-stimulated genes (ISGs) in infected and uninfected cells. The antiviral effector functions triggered by IFN-α/β during a virus infection involve the concerted action of ISGs. In addition to direct innate antiviral factors, ISGs comprise cytokines, chemokines, and molecules associated with antigen presentation (major histocompatibility complex class I), thereby shaping adaptive immune responses (3). The classically studied ISGs, RNase L, PKR, and Mx1, disrupt viral replication and subsequent spread by interfering with both viral and host cell transcription and translation (3, 4). However, the susceptibility to innate antiviral effector mechanisms differs between viruses and may also be distinct between target organs as well as cell types and their differentiation state (4–6). While the role of individual ISGs in reducing viral replication has been characterized for many viruses *in vitro*, their contribution to protection in individual cell types and tissues *in vivo* is not well defined.

The IFN-induced proteins with tetratricopeptide repeats (IFIT) are expressed at very low basal levels but are the most strongly induced ISGs during many viral infections (7–10). There are three *Ifit* family members in mice, *Ifit1* (*Isg56*), *Ifit2* (*Isg54*), and *Ifit3* (*Isg49*), and four in humans, *IFIT1*, *IFIT2*, *IFIT3* (*Isg60*), and *IFIT5* (*Isg58*). Most IFIT functions and antiviral mechanisms were characterized based on *in vitro* analysis of human proteins. Both mouse and human IFIT1 and IFIT2 inhibit protein synthesis by binding to specific translation initiation factor subunits (10–12). Human IFIT1, in heterocomplexes with other IFITs and cellular proteins, also binds and sequesters single-stranded 5′ ppp-RNAs of vesicular stomatitis virus (VSV), thereby inhibiting viral replication (13). Furthermore, analysis of 2′-O-methylation-deficient mutants of corona-, flavi-, and poxviruses demonstrated that IFIT proteins bind to RNAs having specific structures at the 5′ ends (14, 15). However, human IFIT2 can also bind double-stranded RNA without 5′ ppp ends (16). Human IFIT proteins also interact with downstream signaling molecules of the RIG-I/MDA5 pathway (17, 18). Depending on the stimulus and IFIT member, this interaction can suppress, enhance, or have no effect on IFN-α/β induction (17, 18). Amplification of IFN-α/β expression by murine Ifit2 has also just recently been demonstrated in a model of lipopolysaccharide (LPS)-mediated sepsis (19).

The variety of functions perturbed by IFITs *in vitro* (7) suggests numerous potential mechanisms of protection *in vivo*. VSV infection demonstrated that Ifit2, but not Ifit1, displays antiviral activ-

Received 12 August 2013 **Accepted** 30 October 2013
Published ahead of print 6 November 2013
Address correspondence to Cornelia C. Bergmann, bergmac@ccf.org.
† Deceased 17 July 2013.
This paper is dedicated to Niranjan Butchi and his family.

doi:10.1128/JVI.02272-13

ity by preventing VSV spread from the olfactory bulb into the central nervous system (CNS) parenchyma following intranasal infection (20). However, *Ifit2* deficiency did not alter viral replication or pathogenesis following direct intracranial VSV infection. This apparently *Ifit2*-independent VSV spread is likely due to the rapid neuronal replication rate, preventing effective IFN-α/β and ISG induction prior to neuronal death (20). As in VSV infection, Ifit2 also restricts West Nile virus (WNV) infection in specific regions of the brain (21). Furthermore, there is no defect in IFN-α/β production in the CNS following VSV infection of either *Ifit1*$^{-/-}$ or *Ifit2*$^{-/-}$ mice or WNV infection of *Ifit2*$^{-/-}$ mice (20, 21).

Similar to what is observed in other viral CNS infections (22–25), IFN-α/β-mediated innate immune responses are indispensable for controlling neurotropic coronavirus infection (26, 27). Peripheral infection of IFN-α/β receptor-deficient (*Ifnar*$^{-/-}$) mice with the dual liver- and CNS-tropic mouse hepatitis virus (MHV) strain A59 (MHV-A59) results in uncontrolled systemic spread, including to the CNS, and rapid mortality within 2 days (26). Similarly, intracranial infection of *Ifnar*$^{-/-}$ mice with the sublethal, glia-tropic MHV variant JHM (MHV-JHM) results in glial dissemination, expanded tropism to neurons, and mortality within 7 to 8 days (27). Relevant ISGs responsible for IFN-α/β-mediated antiviral activity or neuroprotection during neurotropic coronavirus infections are starting to be studied (6, 14, 28–30). The 2′-5′-oligoadenylate synthetase (OAS)/RNase L pathway, one of the best-characterized innate antiviral mechanisms (31), does not play a significant antiviral role during MHV infection due to rapid degradation of the RNase L-activating oligoadenylates synthesized by activated OAS (30). RNase L deficiency therefore does not affect control of MHV-A59 in the CNS or liver early during infection (6, 30). Similarly, RNase L only modestly prevents spread of the glia-tropic MHV-JHM to CNS microglia/macrophages; nevertheless, it provides protection from fatal disease (28).

The present study assessed the role of Ifit2 as a potential factor contributing to innate antiviral activity during neurotropic coronavirus infection. The results demonstrate that Ifit2 protects against MHV-A59 encephalitis and death by promoting induction of IFN-α/β and *ISG* expression, thereby stemming virus replication and spread within the CNS. The novel role of Ifit2 as a positive regulator of the IFN-α/β pathway during MHV-A59 infection was directly attributed to microglia/macrophages *in vivo* and *in vitro*.

MATERIALS AND METHODS

Mice, viruses, and infections. C57BL/6 mice were obtained from the National Cancer Institute (Frederick, MD). Homozygous *Ifit2*$^{-/-}$ mice on the C57BL/6 background were previously described (20). All mice were housed under pathogen-free conditions at an accredited facility at the Cleveland Clinic Lerner Research Institute and used at 6 to 7 weeks of age. The dually liver-tropic and neurotropic MHV-A59 expressing enhanced green fluorescent protein (EGFP) and the parental wt MHV-A59 were both kindly provided by Volker Thiel, Kantonal Hospital, St. Gallen, Switzerland (32). MHV-A59 expressing EGFP was used throughout, as preliminary experiments confirmed identical *in vivo* and *in vitro* pathogenicity. MHV-A59 was propagated and plaque assayed on delayed brain tumor (DBT) astrocytoma cell monolayers. Mice were infected intracranially in the left hemisphere with 1,000 PFU of MHV-A59 diluted in endotoxin-free Dulbecco's phosphate-buffered saline (PBS) in a final volume of 30 μl. Clinical disease severity was graded daily using the following scale: 0, no disease symptoms; 1, ruffled fur; 2, hunched back/inability to turn upright; 3, severe hunching/wasting/hind limb paralysis; 4, moribund condition or death (33, 34). Intraperitoneal infections were carried out with 1,000 PFU MHV-A59 in 300 μl Dulbecco's PBS. This study was carried out in strict accordance with all provisions of the Animal Welfare Act, the Guide for the Care and Use of Laboratory Animals, and the PHS Policy on Humane Care and Use of Laboratory Animals. All animal experiments were performed in compliance with protocols approved by the Cleveland Clinic Institutional Animal Care and Use Committee (PHS assurance number A3047-01).

Virus titers in the CNS were determined as described previously (27, 28). Briefly, brains and spinal cords were homogenized individually in Dulbecco's PBS using Tenbroeck tissue homogenizers. Homogenates were clarified by centrifugation at 400 × *g* for 7 min at 4°C, and supernatants were stored at −70°C until assayed by plaque assay on DBT astrocytoma cell monolayers as described previously (35).

RNA extraction, reverse transcription, and gene expression analysis. RNA was extracted using TRIzol reagent (Invitrogen, Carlsbad, CA) according to the manufacturer's instructions and subjected to real-time PCR analysis as described previously (34). In brief, snap-frozen tissues were dissociated with TRIzol in a Tissuelyser II (Qiagen, Valencia, CA), treated with chloroform, and RNA was precipitated with isopropyl alcohol, washed with 75% ethanol, and resuspended in RNase-free water (Gibco/Invitrogen, Grand Island, NY). Following treatment with DNase I using a DNA Free kit (Ambion, Austin, TX) for 30 min at 37°C following the manufacturer's instructions, 2 μg RNA was converted to cDNA using the Moloney murine leukemia virus reverse transcriptase (Invitrogen) in buffer containing 10 mM deoxynucleoside triphosphate mix, 250 ng random hexamer primers and oligo(dT) (1:1 ratio) (Invitrogen). cDNA samples were diluted 10-fold in RNase-free water before analysis by quantitative real-time PCR using either SYBR green master mix (Applied Biosystems, Foster City, CA) or TaqMan technology as described previously (36). The primer sequences for SYBR green PCR analysis are as follows: (F, forward; R, reverse): *Gapdh*, F, 5′-CATGGCCTTCCGTGTTCCTA-3′, and R, 5′-ATGCCTGCTTCACCACCTTCT-3′; *Il-6*, F, 5′-ACACATGTTCTCTGGGAAATCGT-3′, and R, 5′-AAGTGCATCATCGTTGTTCATACA-3′; *Nos2*, F, 5′-CCTGGTACGGGCATTGCT-3′, and R, 5′-CATGCGGCCTCCTTTGAG-3′; *Tnf*, F, 5′-GCCACCACGCTCTTCTGTCT-3′, and R, 5′-GGTCTGGGCCATAGAACTGATG-3′; Ccl5, F, 5′-GCAAGTGCTCCAATCTTGCA-3′, and 5′-CTTCTCTGGGTTGGCACACA-3′; *Cxcl9*, F, 5′-TGCACGATGCTCCTGCA-3′, and R, 5′-AGGTCTTTGAGGGATTTGTAGTGG-3′; *Cxcl10*, F, 5′-GACGGTCCGCTGCAACTG-3′, and R, 5′-GCTTCCCTATGGCCCTCATT-3′; and *viral Nucleocapsid*, F, 5′-GCCAAATAATCGCGCTAGAA-3′, and R, 5′-CCGAGCTTAGCCAAAACAAG-3′. All samples were run in duplicate on a 96-well plate using a 7500 fast real-time PCR system (Applied Biosystems) with an automatically set baseline and a manually set critical threshold (CT) at which the fluorescent signal becomes higher than the signals for all of the PCR pairs. Dissociation curves were used to confirm amplification of a single product for each primer pair per sample. Expression levels of *Ccl2*, *Gapdh*, *Ifnα4*, *Ifnα5*, *Ifnβ1*, *Ifnγ*, *Ifit1*, *Ifit2*, *Isg15*, *Il-1β* and *Pkr* were determined using TaqMan primer and probe sets, and 2× universal TaqMan fast master mix (Applied Biosystems). Data were calculated relative to the housekeeping gene *Gapdh* using the following formula: $2^{[CT(\text{GAPDH}) - CT(\text{target gene})]} \times 1{,}000$ (36).

Flow cytometry and fluorescence-activated cell sorting (FACS). Mice were perfused with PBS, and brains were homogenized in 4 ml of Dulbecco's PBS (pH 7.4) using Tenbroeck tissue homogenizers. Following centrifugation at 600 × *g* for 10 min, cell pellets were resuspended in RPMI containing 25 mM HEPES (pH 7.2), adjusted to 30% Percoll (Pharmacia, Uppsala, Sweden) and underlaid with 1 ml of 70% Percoll. Following centrifugation at 800 × *g* for 30 min at 4°C, cells were recovered from the 30%-70% interface, washed with RPMI, and suspended in FACS buffer (0.5% bovine serum albumin in Dulbecco's PBS). Fcγ receptors were blocked with 1% polyclonal mouse serum and 1% rat anti-mouse CD16/

CD32 (clone 2.4G2; BD Biosciences, San Jose, CA) monoclonal antibody (MAb) for 20 min. Specific cell types were identified by staining with fluorescein isothiocyanate (FITC)-, phycoerythrin (PE)-, peridinin chlorophyll protein (PerCP)-, or allophycocyanin (APC)-conjugated MAb for 30 min on ice in FACS buffer. Expression of surface markers was characterized with MAb (all from BD Biosciences except where otherwise indicated) specific for CD45 (clone Ly-5), CD4 (clone GK1.5), CD8 (clone 53-6.7), CD11b (clone M1/70), F480 (Serotec, Raleigh, NC), Ly-6G (clone 1A8), and NK1.1 (clone PK136). Samples were analyzed using a FACSCalibur flow cytometer (BD Biosciences) and FlowJo 7 software (Treestar, Inc., Ashland, OR).

CNS-resident microglia, oligodendroglia, and infiltrating monocytes/macrophages were isolated from brains of infected mice as described previously (36). Briefly, brains from 7 or 8 mice were finely minced and triturated with 0.25% trypsin for 30 min at 37°C. Trypsin was quenched with RPMI containing 20% newborn calf serum; cells were washed in RPMI containing 25 mM HEPES and isolated from the 30%-70% Percoll interface as described above. Following blocking, cells were stained with APC-conjugated anti-CD45 (30-F11), and PE-conjugated anti-F4/80 MAb (Serotec) as described above. CNS-infiltrating $CD45^{hi}$ $F4/80^{+}$ macrophages and resident $CD45^{lo}$ $F4/80^{+}$ microglia were purified on a BD FACSAria cell sorter (BD Biosciences). Oligodendroglia were purified based on their $CD45^{-}$ $O4^{+}$ phenotype following consecutive staining with unconjugated O4 MAb and anti-mouse IgM (FITC) MAb (R6-60.2) (BD Biosciences) as described previously (37, 38). FACS-purified cells were resuspended in TRIzol and stored at −70°C.

Immunohistochemistry and immunofluorescence. Brains from PBS-perfused mice were divided along the midsagittal plane, and one half was fixed with 10% formalin and embedded in paraffin for viral antigen analysis. Viral nucleocapsid protein was identified by immunoperoxidase staining using MAb J3.3 as the primary antibody (39), biotinylated horse anti-mouse IgG as the secondary antibody, and streptavidin-conjugated horseradish peroxidase and 3,3′-diaminobenzidine substrate (Vectastain-ABC kit; Vector Laboratory, Burlingame, CA). High-resolution whole-slide scanning was performed using the Aperio ScanScope digital slide scanner (Carlsbad, CA) with the 40× objective. Sections in each experimental group were evaluated in a blinded fashion, and representative fields were identified.

One half of the brains were embedded in TissueTek O.C.T. compound, flash frozen in liquid nitrogen, and stored at −70°C. Blocks were cut into 10 μm sections in a cryostat at −20°C. Sections were fixed with 4% paraformaldehyde for 20 min at room temperature and permeabilized in 1% Triton-X in PBS for 30 min, and nonspecific antibody binding was blocked using 1% bovine serum albumin and 5% normal goat serum. Cells expressing Ifit2 were identified with rabbit-anti-Ifit2 antibody (20), mouse anti-glial fibrillary acidic protein antibody (GFAP, G-A-5; Sigma-Aldrich, St. Louis, MO), Alexa-fluor 488 conjugated mouse anti-NeuN antibody (MAB377X; Chemicon), and rat anti-CD11b (M1/70; BD Biosciences) in combination with goat anti-rabbit Alexa-fluor 488/594- or goat anti-mouse Alexa-fluor 488/594-conjugated IgG (Invitrogen) as secondary antibodies. Similarly, virus-infected cells were identified using MAb J3.3 (39) and costained for cell type-specific markers with rabbit anti-Iba1 (019-19741; Wako, Richmond, VA), rabbit anti-glial fibrillary acidic protein (Z0334; Dako, Carpinteria, CA), or rabbit anti-NeuN (ABN78; Millipore, Temecula, CA) in combination with the secondary antibodies as described above. Sections were mounted with ProLong Gold antifade mounting medium containing 4′,6-diamidino-2-phenylindole (Invitrogen). Imaging of immunofluorescent sections was performed with a Leica DM4000B fluorescence microscope.

Bone marrow-derived macrophages (BMDM). Mouse bone marrow was obtained flushing femurs and tibiae with BMDM growth medium (Dulbecco's modified Eagle's medium containing 10% fetal calf serum [FCS], 20% L929-conditioned medium as source of colony-stimulating factor 1 (CSF-1), 1% sodium pyruvate, and 0.1% gentamicin). Cells were passed through a 70 μm cell strainer, the concentration was adjusted to 2×10^6 cells/ml in BMDM growth medium, and 20 ml was plated in 75-cm^2 tissue culture flasks for culturing in a humidified, 37°C, 5% CO_2 incubator for 1 week. Cells were washed with DMEM on alternate days to remove nonadherent cells, and fresh BMDM growth medium was added. Cells near confluence were removed by scraping, and 2×10^6 cells were plated into 60-mm by 15-mm petri dishes and incubated for 2 days prior to virus infection. Cells were infected at a multiplicity of infection (MOI) of 1 with MHV-A59 for 1 h at 37°C, unattached virus was removed by washing, and 3 ml DMEM was added prior to incubation in a humidified, 37°C, 5% CO_2 incubator. At various times postinfection (p.i.), cells were lysed directly in 800 μl TRIzol (Invitrogen) and stored at −70°C for RNA isolation as described above. BMDM were confirmed to be >90% $F480^{+}$ and $CD11b^{+}$ cells by FACS analysis.

Nuclear protein fractionation and Western blotting. BMDM (1.2×10^7 cells) were infected with MHV-A59 at an MOI of 10 for 8 or 12 h, resuspended in 750 μl hypotonic buffer (20 mM Tris [pH 8.0], 4 mM $MgCl_2$, 6 mM $CaCl_2$, 0.5 mM dithiothreitol [DTT]). After the addition of 750 μl Dounce lysis buffer (0.6 M sucrose, 0.2% NP-40, 0.5 mM DTT, 10 mM sodium fluoride, 10 mM 2-glycerophosphate), nuclei were released by 20 gentle strokes in 2 ml Dounce homogenizer. Pelleted nuclei (1,000 × *g* for 5 min) were resuspended in glycerol buffer (50 mM Tris [pH 8.3], 5 mM $MgCl_2$, 0.1 mM EDTA, 40% glycerol), washed with PBS, and lysed in 100 μl of lysis buffer (50 mM Tris [pH 8], 150 mM NaCl, 0.2% Triton X-100, 1 mM sodium fluoride, 10 mM 2-glycerophosphate, complete protease inhibitor [Roche]). Whole-cell extracts (6×10^6 cells lysed in 40 μl lysis buffer) and nuclear protein extracts were separated by 4-to-20% gradient SDS-PAGE (Bio-Rad) and transferred to Hybond PVDF membrane (GE Amersham). Membranes were labeled overnight with anti-IRF3 Ab (Santa Cruz sc-9082) and anti-phospho-S396 IRF3 Ab (human S396 = murine S388; Cell Signaling no. 4947). Anti-HDAC1 Ab (Santa Cruz no. sc-7872), anti-actin Ab (Sigma no. A2066), and anti-alpha-tubulin Ab (Sigma no. T6074) were used as loading controls and the control for the absence of cytoplasmic proteins in nuclear fractions, respectively.

Cytokine and chemokine ELISA. Detection of IL-1β and IL-6 in virus infected brain supernatants were performed using mouse IL-1β enzyme-linked immunosorbent assay (ELISA) Ready-Set-Go (eBioscience 88-7013) and IL-6 ELISA Ready-Set-Go (eBioscience 88-7064) according to the manufacturer's instructions. CCL5 in the brain supernatants was measured using mouse CCL5 ELISA kit (MMR00; R&D Systems, Minneapolis, MN) according to the manufacturer's instructions. IFN-γ in brain supernatants was measured by ELISA as described previously (40). Briefly, 96-well plates were coated overnight at 4°C with 100 μl of 0.1 M disodium hydrogen phosphate, pH 9.5, containing 1 μg/ml concentration of purified rat anti-mouse IFN-γ MAb (R4-6A2; BD Bioscience). Nonspecific binding was blocked with 10% FCS in PBS for 1 h, followed by incubation with IFN-γ recombinant cytokine standard (BD Biosciences) and samples at 4°C overnight. Bound IFN-γ was detected using biotinylated rat anti-mouse IFN-γ MAb (XMG1.2; BD Biosciences) and avidin peroxidase followed by 3,3′,5,5′-tetramethylbenzidine (TMB reagent set; BD Biosciences) 30 min later. Optical densities were read at 450 nm with a Bio-Rad model 680 microplate reader and analyzed using Microplate Manager 5.2 software (Bio-Rad Laboratories, Hercules, CA).

IFN-α/β bioassay and serum alanine aminotransferase (ALT) assay. IFN-α/β bioactivity in infected brain homogenates and BMDM supernatants was measured using LL171 cells (kindly provided by Volker Thiel), which are L929 cells stably transfected with an IFN-stimulated response element-luciferase reporter plasmid (ISRE-Luc) (41). Infectious MHV in samples was inactivated by exposure to UV light for 20 min. Recombinant IFN-α A/D (Sigma-Aldrich) was used as a cytokine standard. LL171 cells were grown in opaque 96-well tissue culture-treated plates (Corning, Corning, NY) using DMEM containing 10% FCS and 200 μg/ml G418. Confluent LL171 cells were treated with IFN-α A/D and UV-inactivated samples for 6 h, and luciferase activity was measured with a Spectramax M2 microplate reader after the addition of Bright-Glo luciferase substrate

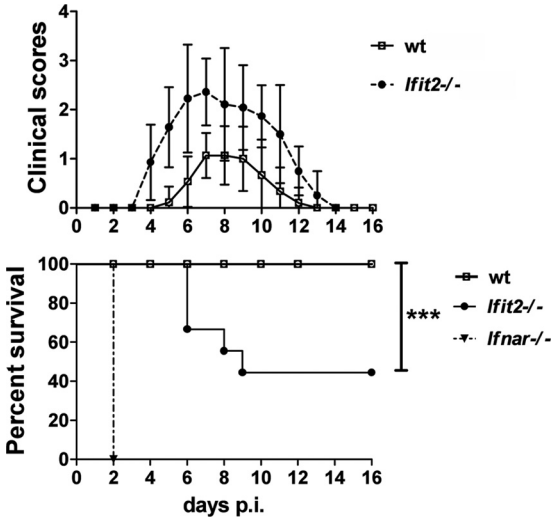

FIG 1 *Ifit2*$^{-/-}$ mice exhibit increased disease severity and mortality. (Top) Morbidity of wt and *Ifit2*$^{-/-}$ mice infected intracranially with 1,000 PFU MHV-A59. Mice were scored daily for clinical disease severity, as described in Materials and Methods. Data are means ± standard deviations and are averages from two independent experiments with 18 to 28 mice/group. Mice which succumbed to infection were not included in clinical scores thereafter. (Bottom) Survival rates of wt, *Ifit2*$^{-/-}$, and *Ifnar*$^{-/-}$ mice infected with 1,000 PFU of MHV-A59. Survival curves, analyzed by the log-rank (Mantel-Cox) test, represent three independent experiments with 10 to 16 mice/group/experiment.

(Promega). IFN bioactivity was calculated using recombinant IFN-α A/D standard dilutions.

ALT activity in serum was measured using an ALT activity assay kit (Sigma-Aldrich) following the manufacturer's instructions.

Statistical analysis. Survival curves were analyzed by a log-rank (Mantel-Cox) test. Real-time PCR data *in vivo* were analyzed by an unpaired, two-tailed Student *t* test. For all *in vitro* studies, statistical analysis was performed by two-way ANOVA using Bonferroni's posttest. Data were analyzed using Prism software (GraphPad Prism5).

RESULTS

Ifit2 protects against neurotropic MHV pathogenesis. Similar to other viral CNS infections (9, 20, 42), *Ifit1* and *Ifit2* are strongly upregulated by neurotropic MHV in an IFN-α/β dependent manner (27, 28). During CNS infections established by VSV and WNV, which both predominantly replicate in neurons, Ifit2 plays a vital protective role, whereas Ifit1 does not appear to contribute to antiviral immunity in adult mice (20, 21). To determine if Ifit2 had a similarly potent protective effect against a neurotropic coronavirus family member with prominent neuron and glia tropism (35), adult *Ifit2*$^{-/-}$ mice were intracranially infected with MHV-A59. The majority of infected wt mice displayed only mild signs of encephalitis with ruffled fur (score of 1); only 10 to 20% of mice exhibited slightly hunched backs (score of 2) starting at day 6 postinfection (p.i.) (Fig. 1). Clinical disease peaked at days 8 to 9 p.i., subsided by day 12 p.i. and was associated with a 100% survival rate. In contrast, disease onset was earlier and morbidity more severe in infected *Ifit2*$^{-/-}$ mice. Clinical disease was evident as early as day 4 p.i. and encephalitis symptoms rapidly progressed in 50% to 60% of *Ifit2*$^{-/-}$ mice as evidenced by severely hunched posture and wasting (score of 3), resulting in mortality between days 6 and 8 p.i. Infected *Ifit2*$^{-/-}$ mice, which reached a clinical score of only 2 (slightly hunched posture) by day 5 p.i., all recovered by day 14 p.i. Very few infected *Ifit2*$^{-/-}$ mice showed hind limb paralysis (<10%). Overall, all *Ifit2*$^{-/-}$ mice that exhibited clinical scores of >2 succumbed to infection, while those with clinical scores of <2 at day 5 p.i. survived, despite higher disease severity than the wt controls during the recovery phase. By comparison, *Ifnar*$^{-/-}$ mice infected with the same virus dose all succumbed to infection by day 2 p.i. (Fig. 1), indicating that other ISGs contribute to early protection in MHV-A59 infection. While a 5-fold increase in virus dose did not alter the survival of wt or the disease phenotype in *Ifit2*$^{-/-}$ mice, a 50-fold increase resulted in 90% mortality in *Ifit2*$^{-/-}$ mice without affecting survival in wt mice (data not shown). These results demonstrate a crucial role of Ifit2 in protection against neurotropic MHV-A59 infection.

Ifit2 suppresses virus replication in the CNS and liver. To elucidate whether disease severity in *Ifit2*$^{-/-}$ mice correlated with uncontrolled viral replication and spread, MHV-A59 replication was measured in the CNS and peripheral tissues (Fig. 2). Infectious virus in brains of wt mice was maximal at days 3 and 5 p.i. but was reduced by ~2 logs by day 7 p.i. (3,930 ± 890 PFU/brain). *Ifit2* deficiency had no impact on initial virus replication at day 3 p.i., but significantly increased infectious virus by day 5 p.i. (Fig. 2A). Closer examination of *Ifit2*$^{-/-}$ mice harboring 2-log-higher levels of virus in the brain revealed they all displayed more severe encephalitis as indicated by clinical scores of >2. Surviving *Ifit2*$^{-/-}$ mice at day 7 p.i. harbored similar virus titers in the brain as wt ALT mice (5,330 ± 1,450 PFU/brain). Analysis of viral nucleocapsid (N) transcripts in the brains confirmed overall higher replication in *Ifit2*$^{-/-}$ mice and supported the correlation between increased virus replication and disease severity (Fig. 2A). The pattern of virus replication in spinal cords of infected *Ifit2*$^{-/-}$ mice mirrored those in the brain at both days 3 and 5 p.i., with significantly higher replication noted at day 5 p.i. relative to wt mice (Fig. 2A).

IFN-α/β mediates protection from uncontrolled MHV-A59 replication in liver, spleen, lungs, and CNS following peripheral infection (26). The dual tropism of MHV-A59 for CNS as well as liver following intracranial infection may thus result in viral spread to peripheral organs, thereby contributing to mortality of *Ifit2*$^{-/-}$ mice. However, after intracerebral infection of adult wt mice, viral mRNA levels in liver and spleen were 20- to 100-fold lower than brains, indicating minimal peripheral replication (Fig. 2A). *Ifit2* deficiency was associated with a modest 2- to 4-fold increase in viral RNA in livers at day 3 p.i. (data not shown), and an ~15-fold increase at day 5 p.i. compared to wt mice (Fig. 2A), supporting an antiviral effect of Ifit2 in the liver. Moreover, elevated levels of viral RNA in livers in individual *Ifit2*$^{-/-}$ mice correlated with elevated levels in the CNS and increased disease severity. Nevertheless, average viral mRNA levels in the livers of *Ifit2*$^{-/-}$ mice were still ~16-fold lower than in the brain, and there was no gross evidence for hepatitis in either wt or *Ifit2*$^{-/-}$ infected mice (data not shown). Furthermore, while serum ALT levels in *Ifit2*$^{-/-}$ mice were slightly higher (41 IU/liter) compared to wt mice (16 IU/liter) at the peak of disease, both were within normal mouse serum ALT ranges (17 to 77 IU/liter), supporting limited liver damage in *Ifit2*$^{-/-}$ mice. There was no evidence for elevated virus replication in spleens of *Ifit2*$^{-/-}$ mice (Fig. 2A). Peripheral intraperitoneal infection also revealed significantly elevated virus replication in the liver of *Ifit2*$^{-/-}$ compared to wt mice at day 5 p.i. (Fig. 2B). However, virus was reduced by day 7 in both groups,

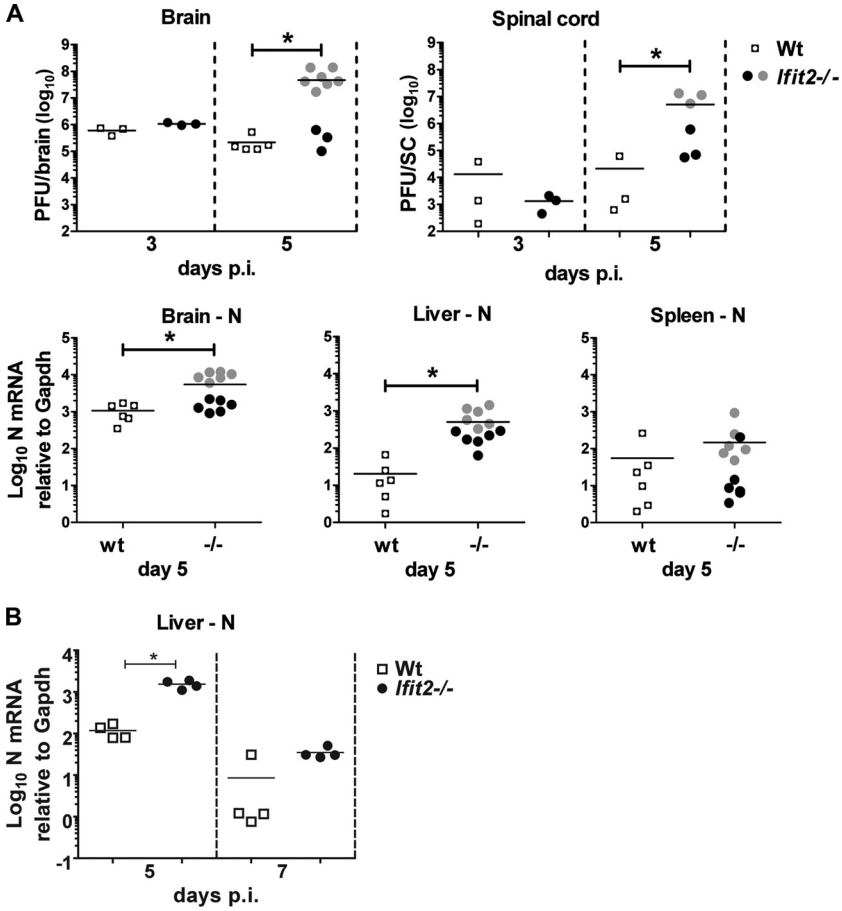

FIG 2 *Ifit2* deficiency increases CNS virus replication in the CNS and liver. (A) Virus load in wt and *Ifit2*$^{-/-}$ mice infected intracranially with MHV-A59. (Top) Virus titers in brain and spinal cord of 3 to 10 mice/group at days 3 and 5 p.i. (Bottom) Quantitative real-time PCR analysis of viral nucleocapsid (N) transcripts at day 5 p.i. in brain, liver, and spleen (6 to 12 mice/group). In the data for day 5 p.i., *Ifit2*$^{-/-}$ mice with severe encephalitis (clinical score > 2) are depicted by solid gray circles. Data are averages from two independent experiments. (B) Wt and *Ifit2*$^{-/-}$ mice infected intraperitoneally with MHV-A59 were assessed for viral N transcripts in liver at days 5 and 7 p.i. by quantitative real-time PCR (4 mice/time point and group). Data in all panels are presented as scatter dot plots with the means indicated; each dot represents one mouse. *, $P < 0.05$. In panel A, data in both portions were analyzed by the unpaired two-tailed Student *t* test, incorporating all mice independent of disease status.

consistent with the absence of clinical symptoms. These data support the notion that Ifit2 provides protection from MHV in both the CNS and liver. Significantly less virus replication in the liver than the brain in wt mice contrasts with results following intracranial infection of young adult 4-week-old mice (6). Differences may reside in various MHV-A59 isolates, inherently increased replication capacity of neuronotropic viruses in the CNS of juvenile mice (43–46) and/or enhanced dissemination from the CNS to visceral organs in young adult mice. Irrespectively, vastly increased morbidity and mortality of *Ifit2*$^{-/-}$ mice following intracranial infection correlated with increased viral replication within the CNS and to a lesser extent with increased peripheral replication.

Ifit2 limits viral spread within the CNS. MHV-A59 infects neurons, and different glial cells in various brain regions, including olfactory bulbs, cortexes, midbrain regions, and brain stems in 4-week-old wt mice (47–49). To determine if Ifit2 preferentially protects a specific brain region or cell type from infection in adult mice, brains were analyzed for distribution of viral antigen at day 5 p.i. The predominant cell type infected in wt mice had the morphology of microglia/macrophages (Fig. 3A), although infected neurons were also easily identified, especially in the brain stem (Fig. 3C and inset). In *Ifit2*$^{-/-}$ mice with severe clinical disease, viral antigen was vastly increased throughout the brain (Fig. 3B), including the cerebellum, which showed minimal infection in wt mice (Fig. 3E and F). While microglia appeared to be the most frequently infected cell type in both wt and *Ifit2*$^{-/-}$ mice, there was a proportionately higher number of infected neurons in the cerebrum (Fig. 3B and inset) and brain stem (Fig. 3D and inset) of *Ifit2*$^{-/-}$ mice. In the cerebellums of *Ifit2*$^{-/-}$ mice, numerous neurons were infected in the molecular and granular cell layers, with some of the infected neurons forming small foci (Fig. 3F and inset). The increased number of virus infected cells throughout the brain in *Ifit2*$^{-/-}$ mice correlated with higher virus load compared to wt counterparts.

Cell type-specific markers were used to more precisely determine potential preferences in cellular tropism. In both wt and *Ifit2*$^{-/-}$ mice, virus was readily detected in neurons (NeuN^{+}) and microglia/macrophages (Iba1^{+}) but not in astrocytes (GFAP^{+}) (Fig. 4A to C). The absence of infected astrocytes in the present study contrasts with MHV-A59 infection of 4-week-old mice (6). This discrepancy may be due to different MHV-A59 isolates or

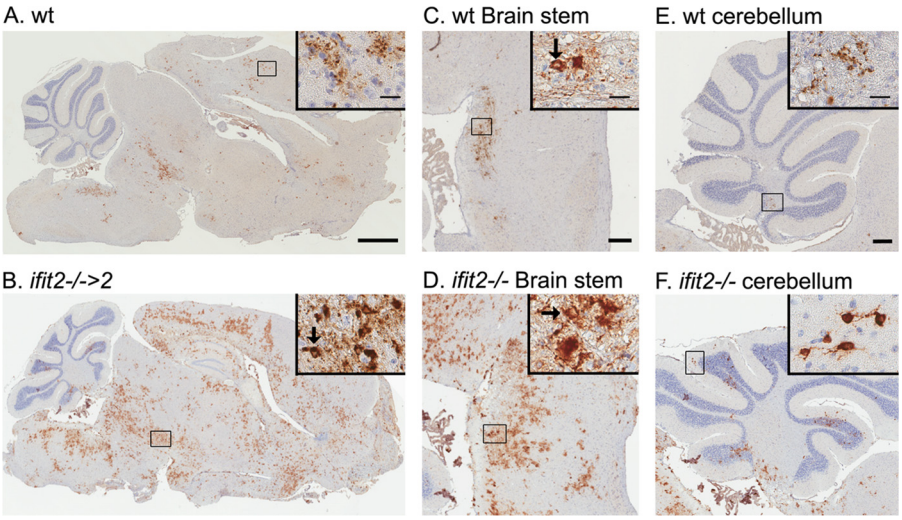

FIG 3 *Ifit2* deficiency enhances virus dissemination. Viral antigen in brains of infected wt (A, C, and E) and *Ifit2*$^{-/-}$ (B, D, and F) mice (clinical score > 2) at day 5 p.i. detected by immunoperoxidase staining using monoclonal antibody J3.3 specific for viral N protein (red chromogen; hematoxylin counterstain). Note increased foci of viral antigen-positive cells in the cerebrum (A and B) of *Ifit2*$^{-/-}$ mice. Brain stem (C and D) and cerebellum (E and F) from wt (top) and *Ifit2*$^{-/-}$ (bottom) mice. Insets show infected cells at higher magnifications; arrows point to cells with neuronal morphology. Bars, 1,000 μm (A and B), 250 μm (C to F), and 20 μm (all insets).

host age-related differences, as indicated above (43–46). Additional analysis of viral RNA in oligodendroglia, microglia, and macrophages purified by FACS indicated that the relative increase in viral mRNA in *Ifit2*$^{-/-}$ over wt cells was similar in all populations, ranging from 1.6- to 2.5-fold higher levels (Fig. 4D). These results suggest that Ifit2 is protective against MHV-A59 infection in various CNS cell types *in vivo*, and its effects are most evident in the cerebellum and brainstem. Moreover, the focal small groups of neurons infected in the cerebellum (Fig. 3F and inset) suggest the possibility of enhanced neuron-to-neuron transmission in the absence of *Ifit2*.

Ifit2 deficiency results in impaired IFN-α/β and ISG induction in the CNS. IFIT proteins can interfere directly with viral replication by disrupting translation or indirectly by interfering with RIG-I/MDA5 signaling altering downstream IFN-α/β production (12, 13, 17, 18). Although the latter has been observed

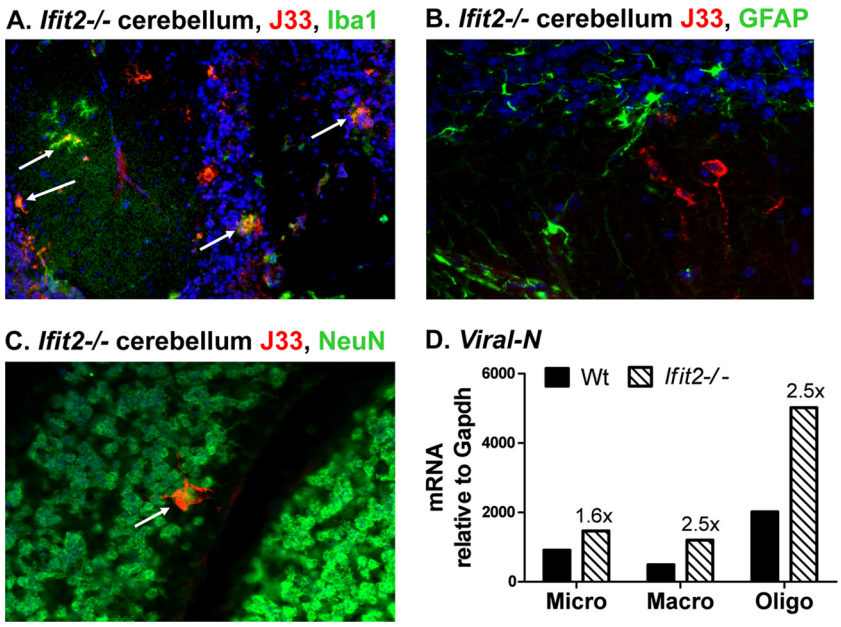

FIG 4 *Ifit2* deficiency enhances virus replication in microglia/macrophages and in neurons in the hind brain. Virus-infected cells in *Ifit2*$^{-/-}$ brains at day 5 p.i. were stained with the anti-N antibody J3.3 (A to C; red), and costained with anti-Iba1 (A; green), anti-GFAP antibody (B; green), or anti-NeuN (C; green). Data are representative of three individual mice with clinical scores of >2. (D) Expression of viral N protein transcripts in microglia (Micro), macrophages (Macro), and oligodendroglia (Oligo) purified from infected brains by FACS at day 4 p.i. Data represent 10 mice per sample. Numbers above the bars are fold increase compared to wt.

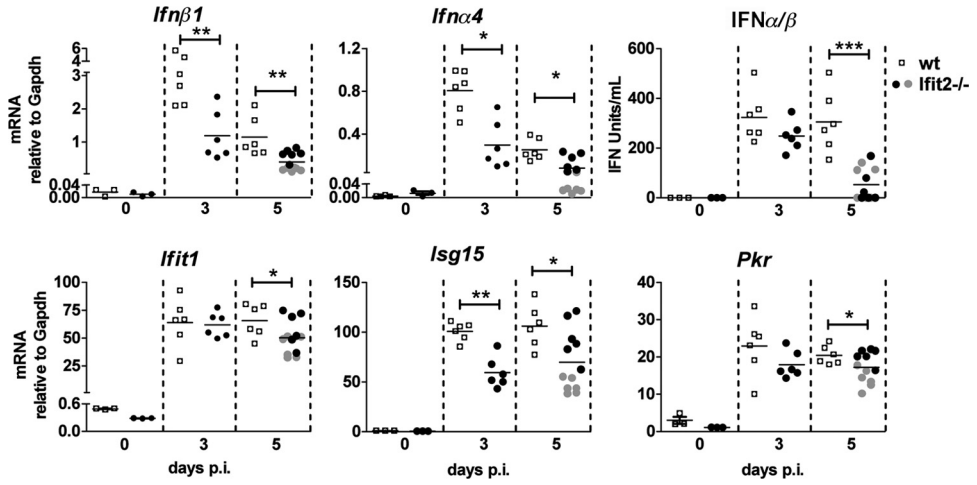

FIG 5 Reduced expression of IFN-α/β and ISG in the absence of *Ifit2*. Expression of *Ifn*β*1*, *Ifn*α*4*, *Ifit1*, *Isg15*, and *Pkr* mRNA and IFN activity in brains of wt and *Ifit2*$^{-/-}$ mice at days 0, 3, and 5 p.i. (3 to 12 mice/group/time point). IFN-α/β activity in brain supernatants was measured by an IFN-sensitive luciferase reporter assay (top, right). Data were analyzed by the unpaired two-tailed Student *t* test and are means ± standard errors of the means for 3 replicates representative of 3 independent experiments. Vertical lines separate data from the indicated days p.i. Data from two independent experiments were analyzed by the unpaired two-tailed Student *t* test and are presented as scatter dot plots with the means indicated; each dot represents a different mouse. In the data for day 5 p.i., *Ifit2*$^{-/-}$ mice with severe encephalitis (clinical score > 2) are depicted by solid gray circles. *, $P < 0.05$; **, $P < 0.01$; ***, $P < 0.005$.

only with human IFIT family members (17, 18), Ifit2-mediated amplification of IFN-α/β was recently observed in a murine endotoxin shock model (19). Coronaviruses, including MHV-A59, induce IFN-α/β in microglia/macrophages via MDA5 (50). Furthermore, IFN-α/β signaling on macrophages and dendritic cells is critical for the early containment of MHV within secondary lymphoid organs (51). To ensure that uncontrolled virus replication was not due to impaired IFN-α/β production, expression of *Ifn*-α/β mRNA in the brains of *Ifit2*$^{-/-}$ mice was compared to that in wt mice. Surprisingly, *Ifn*-α*4* and *Ifn*-β*1* mRNA expression was significantly reduced in *Ifit2*$^{-/-}$ relative to wt mice at both days 3 and 5 p.i. (Fig. 5). Moreover, at day 5 p.i., the decrease in *Ifn*-α/β mRNA was most pronounced in *Ifit2*$^{-/-}$ mice with clinical scores of >2 and high viral loads (~10-fold) compared to wt controls (Fig. 5). IFN levels in brain homogenates measured by IFN-α/β bioassay were also significantly reduced in *Ifit2*$^{-/-}$ mice compared to wt controls at day 5 p.i., although differences were not significant at day 3 (Fig. 5). Impaired IFN-α/β was supported by significantly reduced expression of mRNA encoding the downstream ISGs *Ifit1*, *Isg15*, and *Pkr* compared to wt controls (Fig. 5). Reduced expression of IFN-α/β and ISG mRNAs was also observed in spinal cords of infected *Ifit2*$^{-/-}$ mice harboring high virus loads relative to wt mice (data not shown). These results suggest that the absence of *Ifit2* impairs IFN-α/β expression at the preclinical stage, when viral replication was still similar in both groups. Limited IFN-α/β subsequently reduces ISG induction and contributes to increased virus replication, which in turn further impairs IFN-α/β expression at later times p.i. These data support a novel *Ifit2*-mediated positive feedback loop in propagating IFN-α/β induction during MHV CNS infection.

Increased viral replication is generally associated with enhanced expression of proinflammatory cytokines and chemokines, which are partially regulated by activation of pattern recognition receptors. As MHV-A59 induces IFN-α/β via MDA5 signaling (50), we assessed whether *Ifit2* deficiency specifically affected the IFN-α/β pathway or also modulated induction of proinflammatory cytokines and chemokines. Ifit2 deficiency did not alter mRNA expression of the acute-phase proinflammatory cytokines IL-6, NOS2, and TNF and only modestly reduced IL-1β mRNA at day 5 p.i. (Fig. 6). In addition, expression of mRNA encoding the macrophage or lymphocyte chemoattractants CCL2, CCL5, CXCL9, and CXCL10 were similar in infected *Ifit2*$^{-/-}$ mice relative to wt mice (Fig. 6). In contrast, mRNA expression of IFN-γ, a cytokine prominently released by T cells and critical for controlling virus in oligodendroglia (52), was increased in *Ifit2*$^{-/-}$ mice, consistent with enhanced T cell stimulation by increased virus load (Fig. 6). As Ifit2 may inhibit protein translation (10), expression of proinflammatory cytokines and chemokines was measured by ELISA. *Ifit2*$^{-/-}$ mice bearing higher virus loads exhibited similar levels of IL-1β and IL-6 and slightly reduced CCL5 levels but increased IFN-γ levels compared to wt mice (Fig. 7). These protein patterns reflected mRNA levels and suggested no major role for Ifit2 in global translational inhibition *in vivo*. Characterization of cells recruited to the CNS by flow cytometry also revealed similar total numbers of infiltrating cells and no alterations in their composition (data not shown). Neutrophils comprised the most prominent population at day 3 p.i., and macrophages peaked at day 5 p.i. in both groups. Slightly higher numbers of infiltrating CD8 T cells in *Ifit2*$^{-/-}$ brains with severe disease at day 5 p.i. coincided with increased IFN-γ and supported intact adaptive immune responses in these mice (data not shown). Overall, these results demonstrate that Ifit2 deficiency specifically impairs induction of IFN-α/β but not proinflammatory cytokines or chemokines.

Kinetics and cell type-specific *Ifit2* expression. Predominant induction of IFN-α/β in microglia/macrophages following MHV-A59 CNS infection (50) implicated a specific role for Ifit2 in myeloid cells. We therefore assessed the kinetics of *Ifit2* gene mRNA expression in relation to IFN-α/β and characterized the prominent cell types inducing Ifit2 protein. Consistent with maximal expression of IFN-α/β mRNA at day 3 p.i., *Ifit2* transcripts were strongly induced by this time (Fig. 8A). Moreover, although IFN-

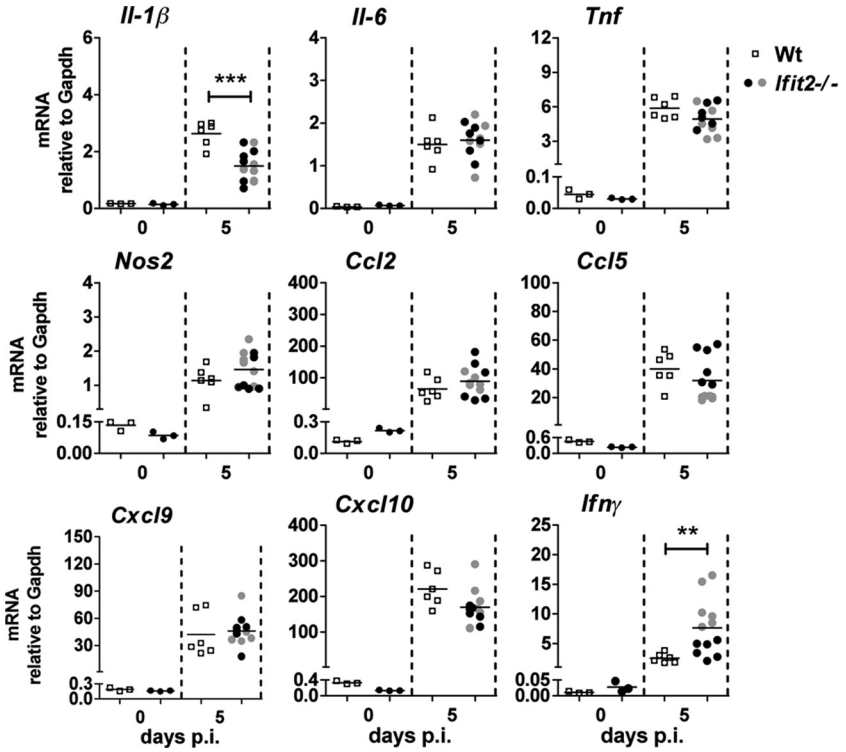

FIG 6 *Ifit2* deficiency does not regulate mRNA expression of proinflammatory cytokines and chemokines. Expression of *Il-1*β, *Il-6*, *Tnf*, *Nos2*, *Ccl2*, *Ccl5*, *Cxcl9*, *Cxcl10*, and *Ifn*γ mRNA in brains of wt and *Ifit2*$^{-/-}$ mice at days 0 and 5 p.i. (3 to 12 mice/group/time point) is shown. The vertical line separates data from the different days p.i. Data from two independent experiments were analyzed by the unpaired two-tailed Student *t* test and are presented as scatter dot plots with the means indicated; each dot represents a different mouse. In the data for day 5 p.i., *Ifit2*$^{-/-}$ mice with severe encephalitis (clinical score > 2) are depicted by solid gray circles. *, $P < 0.05$; ** $P < 0.01$; ***, $P < 0.005$.

α/β mRNA gradually declined to basal levels by day 7 p.i., *Ifit2* mRNA levels were sustained until day 5 p.i. and only gradually declined. At day 10 p.i., *Ifit2* mRNA levels were still significantly higher than naive levels (Fig. 8A).

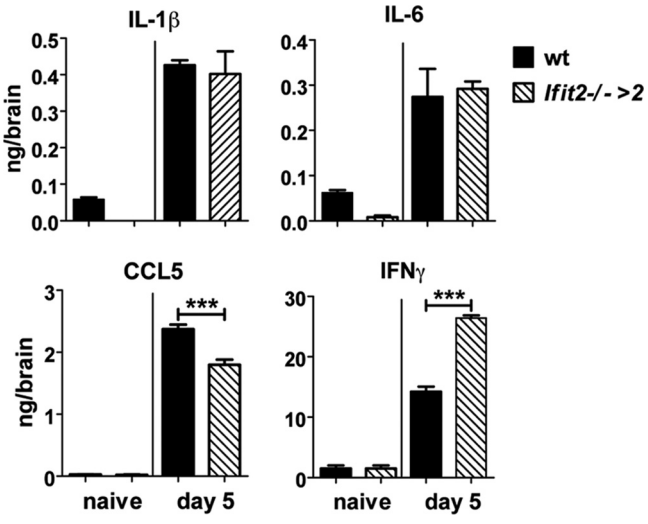

FIG 7 *Ifit2* deficiency does not impair inflammatory cytokines and chemokines. IL-1β, IL-6, CCL5, and IFN-γ in brain supernatants of individual infected wt and *Ifit2*$^{-/-}$ mice (clinical score > 2) at day 5 p.i. measured by ELISA (3 to 6 mice/group). Data were analyzed by the unpaired two-tailed Student *t* test. Data are means and standard errors of the means. ***, $P < 0.001$.

The relative kinetics and expression of *Ifit2* mRNA were also quantitated in FACS-purified microglia (CD45^{lo} F4/80^{+}), oligodendroglia (O4^{+}), and CNS-infiltrating monocytes/macrophages (CD45^{hi} F4/80^{+}). *Ifit2* mRNA was expressed in all three cell types at day 3 p.i., reached maximal levels at day 5 p.i., and declined by day 7 p.i. (Fig. 8B). Infiltrating macrophages expressed *Ifit2* mRNA at increased levels compared to resident microglia and oligodendroglia. Peak *Ifit2* mRNA expression correlated kinetically with the prominent effect of *Ifit2* deficiency on virus replication at day 5 p.i.

To analyze the anatomical localization of Ifit2 protein (p54) in relation to virus distribution, brain sections from wt mice were costained for Ifit2 and viral protein. Ifit2 was detected in ependymal cells, the choroid plexus, and the brain parenchyma proximal to ventricles, as well as in focal areas within olfactory bulbs, the cortex, and midbrain regions (data not shown). Moreover, in all these regions, Ifit2 was found within and adjacent to infected cells, suggesting IFN-α/β-mediated induction in both infected and proximal uninfected cells (Fig. 8C). The predominant cells expressing Ifit2 were neurons and microglia/macrophages, the major cell types infected during acute disease (Fig. 8C). In contrast, Ifit2 was not detected in astrocytes (GFAP^{+}) (Fig. 8C), although astrocytes are capable of responding to IFN-α/β and IFN-γ (53–55). The identity of Ifit2-expressing cells not costaining for CD11b, GFAP, or NeuN markers remains unknown. However, both nonactivated and modestly activated microglia expressing low levels of CD11b and oligodendrocytes are likely candidates.

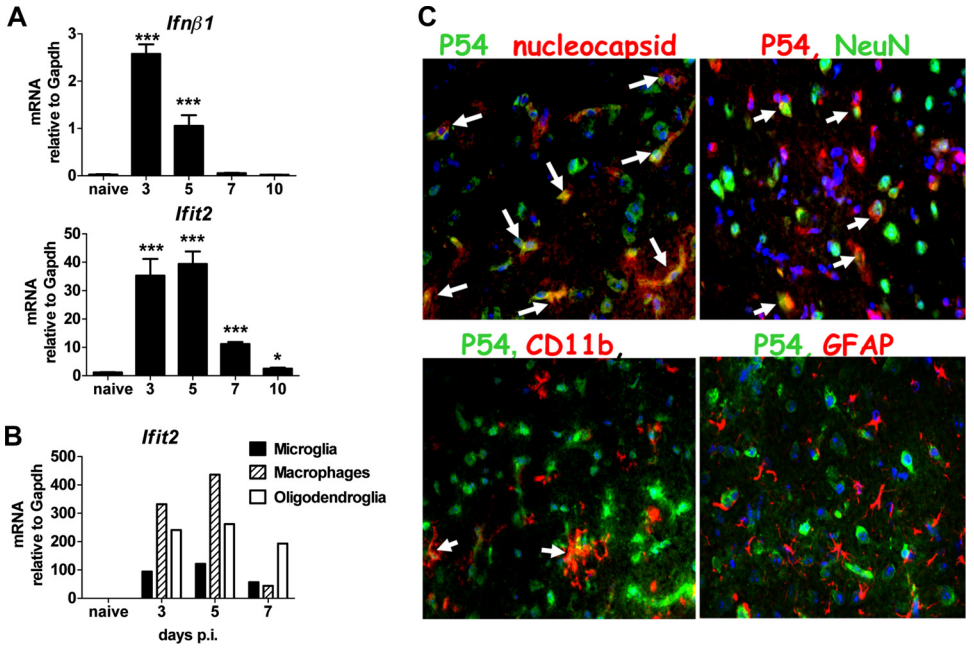

FIG 8 *Ifit2* induction in response to MHV-A59 infection. (A) Expression of *Ifn*β*1* and *Ifit2* in brains of infected wt mice at indicated time points p.i. Data were analyzed by the unpaired two-tailed Student *t* test and are means and standard errors of the means for 7 mice from two independent experiments. *, $P < 0.05$; ***, $P < 0.001$. (B) *Ifit2* mRNA levels in microglia, macrophages, and oligodendroglia purified from brains of naive or infected wt mice at the indicated time points. Data represent a single experiment with 10 pooled mice per time point. (C) Colocalization of Ifit2 protein (P54) with virus infected cells (N; red), microglia/macrophages (CD11b; red), neurons (NeuN; green), and astrocytes (GFAP; red) in brains of wt mice at day 5 p.i. Data are representative of three individual mice.

Overall, these data confirmed prominent Ifit2 expression in cell types known to induce IFN-α/β.

Ifit2 deficiency impairs IFN-α/β and ISG expression in microglia and macrophages. CNS resident microglia and infiltrating macrophages are the major source of MDA5-dependent IFN-α/β induction following MHV infection, whereas neurons, oligodendroglia, and astrocytes do not produce IFN-α/β (36, 50). Impaired *Ifn*-α/β mRNA expression in the CNS of infected *Ifit2*$^{-/-}$ mice was thus most likely attributed to impaired IFN-α/β expression in microglia or macrophages. This was verified by RNA analysis of microglia and CNS-infiltrating monocytes/macrophages purified from infected brains at days 4 and 5 p.i., correlating with onset of clinical signs and impaired IFN-α/β expression in *Ifit2*$^{-/-}$ mice. At day 4 p.i., mice were selected unbiasedly for cell preparations, as wt mice exhibited no clinical disease and *Ifit2*$^{-/-}$ mice exhibited only very mild symptoms. However, as 50 to 60% of *Ifit2*$^{-/-}$ mice progressed to severe disease by day 5 p.i., *Ifit2*$^{-/-}$ mice were segregated into moderately and severely diseased groups to determine if expression patterns in monocytes/macrophages and microglia reflected clinical disease. Both microglia and macrophages from *Ifit2*$^{-/-}$ mice expressed higher levels of viral mRNA at day 4 p.i. but reduced levels of *Ifn*β*1*, *Ifn*α*4*, and *Ifn*α*5* mRNA relative to wt counterparts (Fig. 9). Although *Ifn*β*1* mRNA levels were only marginally reduced in *Ifit2*$^{-/-}$ microglia, *Ifn*α*4* and *Ifn*α*5* mRNA levels were reduced 5-fold and 3-fold, respectively. Monocyte/macrophages from *Ifit2*$^{-/-}$ mice at day 4 p.i. revealed slight differences in the extent of the relative *Ifn*-α/β mRNA decrease. Increasingly impaired *Ifn*-α/β mRNA expression with increased viral load became even more evident by day 5 p.i. (Fig. 9). *Ifn*-α/β mRNA levels were reduced more severely in *Ifit2*$^{-/-}$ microglia and macrophages harboring high viral mRNA compared to both wt and *Ifit2*$^{-/-}$ counterparts from mice with mild encephalitis (Fig. 9). Decreased *Ifn*-α/β mRNA levels at day 5 p.i. compared to day 4 p.i. support the concept that an early reduction in IFN-α/β leads to increased virus replication. Similarly, mRNA expression of the ISG *Ifit1*, *Isg15*, and *Pkr* was reduced 1.5- to 2.5-fold in both microglia and macrophages (data not shown). In contrast, mRNA expression of the monocyte chemoattractant CCL2 (56) was not altered in *Ifit2*$^{-/-}$ microglia or macrophages by day 4 p.i. (Fig. 9) and even increased in microglia from *Ifit2*$^{-/-}$ mice with severe encephalitis compared to wt counterparts. Nevertheless, *Ccl2* mRNA levels declined severely in macrophages. Reduced IFN-α/β expression within the CNS in the absence of *Ifit2* is thus attributed to both microglia and CNS-infiltrating macrophages.

As the infection rate of microglia/macrophages *in vivo* is low, based on histological analysis, BMDM were utilized to assess the effect of Ifit2 on virus replication and IFN-α/β expression following MHV-A59 infection *in vitro*. Kinetic analysis of infected wt BMDM revealed that viral mRNA peaked at 12 and was maintained until 18 h p.i., whereas *Ifn*-α/β mRNA expression peaked at 18 h p.i. Expression of *Ifn*-α/β and ISG mRNAs was thus compared at 12 and 18 h p.i. Viral mRNA levels in *Ifit2*$^{-/-}$ BMDM were not significantly different from those in wt BMDM, suggesting no direct effects of Ifit2 on virus replication (Fig. 10). However, *Ifn*-β*1* mRNA levels in infected *Ifit2*$^{-/-}$ BMDM were reduced ~90-fold and ~60-fold at 12 and 18 h p.i., respectively (Fig. 10). Expression of *Ifn*-α*4* and *Ifn*-α*5* mRNA was reduced even more robustly than that of *Ifn*-β*1* mRNA in *Ifit2*$^{-/-}$ relative to wt BMDM at 18 compared to 12 h p.i., reflecting *Ifn*-α*4* and *Ifn*-α*5* amplification in wt but not *Ifit2*$^{-/-}$ cells. Furthermore, IFN-α/β

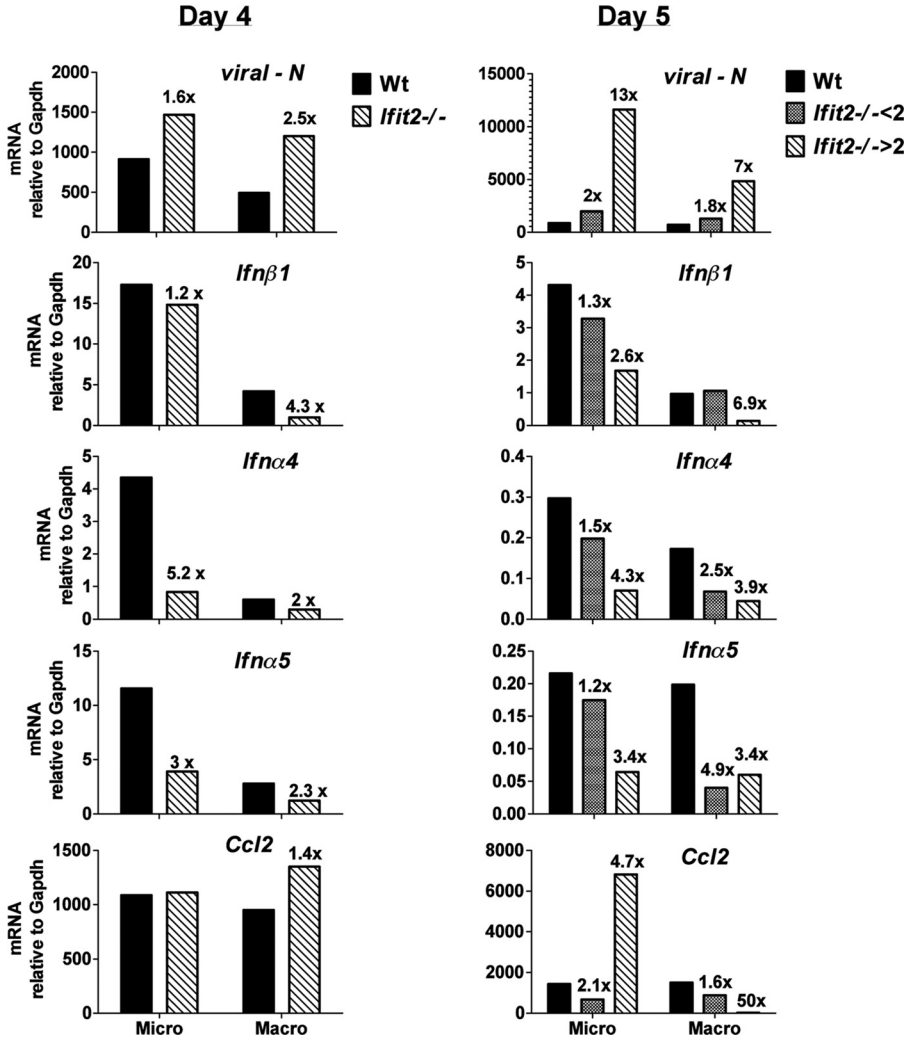

FIG 9 *Ifit2* deficiency impairs *Ifn*α/β expression in microglia and macrophages. CD45^{lo} F480^{+} microglia (Micro) and CD45^{hi} F480^{+} macrophages (Macro) purified from infected wt and *Ifit2*$^{-/-}$ brains at day 4 p.i. (left) and 5 p.i. (right) by FACS were compared for expression of viral N, *Ifn*β*1*, *Ifn*α*4*, *Ifn*α*5*, and *Ccl2* mRNAs. For day 5 p.i., samples were cell preparations from *Ifit2*$^{-/-}$ mice with moderate encephalitis (scores ≤ 2) and severe encephalitis (scores > 2). Data represent one experiment with 6 to 10 pooled mice per group and per time point. Numbers above the bars are fold differences compared to the wt.

in *Ifit2*$^{-/-}$ BMDM supernatants was barely detectable (<3 U/ml) compared to wt macrophage supernatants (18 to 20 U/ml) at 12 h p.i. (Fig. 10), reflecting impaired *Ifn*-α/β transcript expression. The downstream ISG *Ifit* and *Isg15* mRNAs were also reduced 10- to 20-fold in the *Ifit2*$^{-/-}$ compared to wt BMDM, albeit to a lesser extent than the IFN-α/β genes. In contrast, mRNA expression of the proinflammatory cytokine TNF and chemokine CCL2 was only modestly reduced in *Ifit2*$^{-/-}$ BMDM (Fig. 10). This confirmed the preferential impairment in IFN-α/β induction compared to NF-κB dependent genes observed in the infected brain. Impaired *Ifn*-α/β and ISG mRNA expression in *Ifit2*$^{-/-}$ BMDM, with no difference in viral replication, supports a direct role of Ifit2 in promoting the IFN-α/β pathway rather than interfering with viral replication at the translational level.

Ifit2 deficiency impairs virus-induced IRF3 phosphorylation in BMDM. Both human IFIT3 and murine Ifit2 have been shown to enhance IFN-α/β induction and amplification by upregulating IRF3 phosphorylation (18, 19). IFIT3 exerts its function by bridging mitochondrial antiviral signaling protein (MAVS), the adapter for MDA5/RIG-I signaling, with the IRF3 kinase TBK1 (18). As MDA5 is essential in inducing IFN-α/β following MHV infection in macrophages/microglia, MHV-A59-infected wt and *Ifit2*$^{-/-}$ BMDM were assessed for potential alterations in IRF3 modification. Immunoblotting of whole-cell lysates with anti-IRF3 Ab indicates that overall modification of IRF3 is independent of Ifit2 following 8 or 12 h p.i. Translocation of the modified IRF3 forms into the nucleus is also similar (Fig. 11). Nevertheless, use of a phospho-specific MAb to assess IRF3 phosphorylation at serine (S) residue 388, which marks the site most critical for transcriptional activity (57), revealed a limited phosphorylation specifically at this site in both whole-cell lysates and nuclear extracts. These data support the idea that limited S388 phosphorylation of IRF3 in the absence of Ifit2 may contribute to reduced IFN-α/β expression following MHV infection.

DISCUSSION

The contribution of individual ISGs to IFN-α/β-mediated innate immune control of coronavirus infections is not well understood.

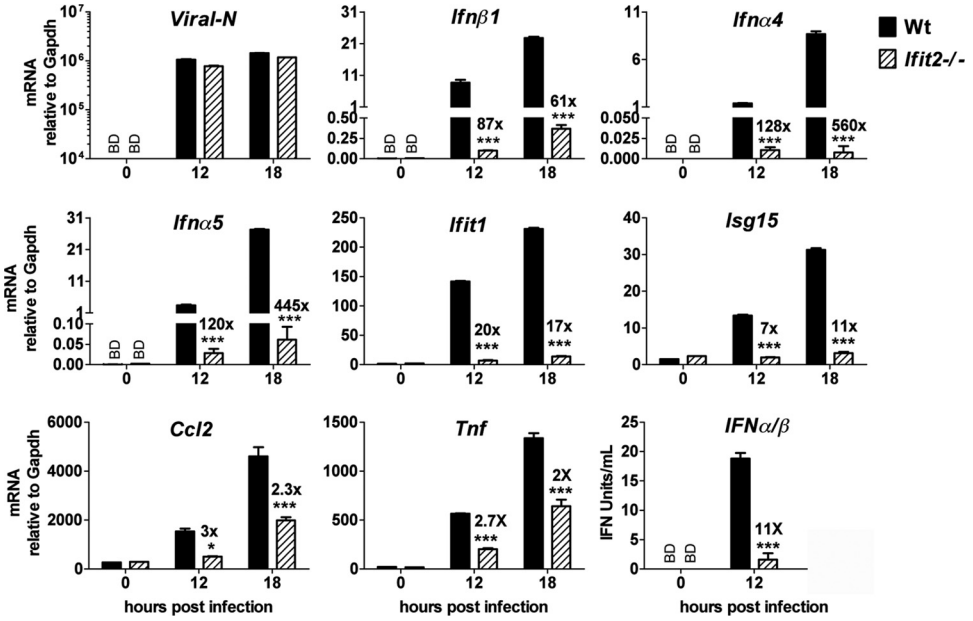

FIG 10 Impaired *in vitro* induction of IFN-α/β and ISG but not cytokine expression in the absence of *Ifit2*. BMDM cultures from wt and *Ifit2*$^{-/-}$ mice were infected with MHV-A59 at an MOI of 1. Expression of viral N, *Ifnβ1*, *Ifnα4*, *Ifnα5*, *Ifit1*, *Isg15*, *Ccl2*, and *Tnf* mRNA were measured at 12 and 18 h p.i. IFN-α/β activity in culture supernatants from infected wt or *Ifit2*$^{-/-}$ BMDM was measured by an IFN-sensitive luciferase reporter assay. Data were analyzed by the unpaired two-tailed Student *t* test and are means and standard errors of the means for 3 replicates representative of three independent experiments. Numbers above the bars are fold decreases compared to the wt. **, $P < 0.01$; *** $P < 0.001$. BD, below the limit of detection.

The classically studied OAS/RNase L pathway is antiviral in many RNA viral infections, including coxsackievirus, encephalomyocarditis virus (EMCV), and WNV (58–60), but does not exert prominent antiviral activity following MHV infection (28). This was recently attributed to a virally encoded protein which actively degrades oligoadenylates, which are essential to activate RNase L (30). Nevertheless, despite only modestly affecting MHV replication in microglia/macrophages *in vivo*, RNase L dampens and delays virus-induced demyelination (28). The IFIT proteins are among the most strongly induced ISGs following MHV infection (27, 28), similar to many other viral infections (9). The present study revealed induction of Ifit2 in infected and proximal uninfected cells, supporting the idea that Ifit2 expression is confined to regional areas of virus replication within the CNS. Moreover, analysis of *Ifit2*$^{-/-}$ mice identified Ifit2 as a major antiviral ISG limiting MHV replication in the CNS and liver and preventing both viral CNS dissemination and mortality.

Infection with a viral dose resulting in 100% mortality in *Ifnar*$^{-/-}$ mice within 2 days p.i. resulted in a delayed 60% mortality rate in *Ifit2*$^{-/-}$ mice, while wt mice all survived. Mortality in *Ifit2*$^{-/-}$ mice correlated with increased CNS virus replication as well as spread to the cerebellum and brainstem, which were minimally infected in wt mice. Although *Ifit2* also displayed antiviral activity in the liver, reduced overall viral RNA levels in liver compared to brains of *Ifit2*$^{-/-}$ mice and no gross evidence for hepatitis suggested a limited contribution of peripheral infection to morbidity and mortality. The absence of overt liver damage was further supported by lack of enhanced serum ALT levels in intracranially infected *Ifit2*$^{-/-}$ compared to wt mice. Analysis of cellular tropism revealed no indication of preferential action of Ifit2

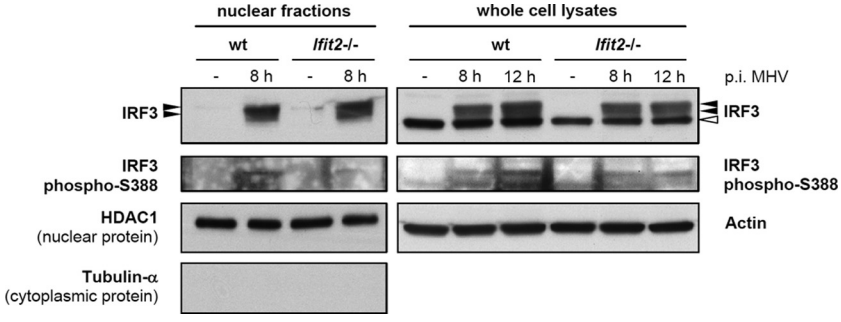

FIG 11 IRF3 phosphorylation and nuclear translocation in wt and *Ifit2*$^{-/-}$ BMDM. Nuclear protein fractions and whole-cell lysates of MHV-A59-infected BMDM were subjected to immunoblotting at the indicated time points to detect latent IRF3 (white arrowhead), virus-induced IRF3 posttranslational modification (black arrowheads), nuclear translocation, and serine 388 phosphorylation. Purity of nuclear extracts was confirmed by the absence of strictly cytoplasmic tubulin-α. Data are representative of two separate experiments with similar results.

within distinct CNS cell types. Similar to wt mice, astrocytes were not infected in *Ifit2*$^{-/-}$ mice. Microglia/macrophages constituted the most common cell type infected in both wt and *Ifit2*$^{-/-}$ mice, including in the brain stem and cerebellum. The lack of astrocyte infection and minimal liver infection in wt mice contrasts with pathogenesis studies in younger (4-week-old) mice (6), possibly due to use of distinct MHV-A59 isolates or host age-related differences (43–46). Irrespectively, the proportionately higher number of infected neurons in brain stem suggested that mortality of *Ifit2*$^{-/-}$ mice may be due to cardiorespiratory failure. Furthermore, the spread of MHV to the cerebellum and brainstem may be attributed to similar mechanisms underlying Ifit2-mediated restriction of VSV neuronal spread following intranasal infection (20). This notion is supported by the small foci of infected neurons in the cerebellum.

The mechanism by which Ifit2 exerts antiviral activity remains to be elucidated. A role of Ifit2 in supporting IFN-α/β induction and amplification is indicated by reduced IFN-α/β and ISG mRNA levels, as well as reduced IFN-α/β activity, in the CNS of *Ifit2*$^{-/-}$ mice even prior to symptomatic disease. Coronaviruses, including MHV-A59, are overall poor type I IFN inducers due to 2′-O-methylation of their capped mRNA (15), which disguises viral RNAs and prevents recognition by MDA5 (15). Nevertheless, macrophages and microglia infected with MHV do induce IFN-α/β via MDA5 signaling (50), and IFN-α/β responsiveness by macrophages is critical to contain viral spread (51). Reduced IFN-α/β in the CNS of *Ifit2*$^{-/-}$ mice was indeed directly attributed to myeloid cells, which are the prominent source of IFN-α/β within the MHV-infected CNS (36, 50). Together, the above data strongly imply that Ifit2 deficiency affects an MDA5-dependent pathway of IFN-α/β induction (15, 17, 50). MDA5 signaling recruits the downstream adaptor proteins TRAF3 or TRAF6 and the kinases TBK1 and IKKα/β to the MAVS complex, thereby inducing IRF3/IRF7-mediated IFN-α/β and NF-κB-mediated cytokine expression (61). Reduced IRF3 S388 phosphorylation in MHV-infected BMDM lysates in the absence of Ifit2 supported a correlation between Ifit2 and IRF3 activation, as suggested by the drastic reduction in both *Ifn*-α/β mRNA and secreted protein in infected *Ifit2*$^{-/-}$ compared to wt BMDM. Furthermore, both microglia and infiltrating monocytes purified from the infected CNS expressed reduced *Ifn*-α/β mRNA levels despite elevated viral mRNA in the absence of *Ifit2*. As *Ifit2* is itself an ISG, early IFN-α/β induction would promote Ifit2-enhanced IRF3 transcriptional activation in a positive feedback loop. A role of Ifit2 in amplifying IFN-α/β via enhanced IRF3 transcriptional activity is in agreement with a recent publication linking the absence of Ifit2 with reduced IRF3 phosphorylation and consequently reduced IFN-α/β induction in a TLR4 stimulated sepsis model (19). This notion is also supported by IFIT3-mediated potentiation of IFN-α/β induction following VSV, Sendai virus, and influenza A virus infection by bridging TBK1 and the upstream adapter MAVS molecules in the RIG-I/MDA5 pathway (17, 18). A subtle yet critical signaling threshold set early by the level of IRF3 activation in MHV-A59 *Ifit2*$^{-/-}$ mice may thus contribute to the diverging CNS viral control and pathogenesis.

Reduced IRF3 phosphorylation in the absence of Ifit2 may further be exacerbated by MHV-derived decoy proteins competing for TBK1, as shown for the paramyxovirus V protein (62). In this context, it is interesting that the MHV nucleocapsid protein is phosphorylated at several S residues, although the cellular kinases have not been identified (63, 64). The MHV-A59 papain-like protease domain 2 of the nonstructural protein 3 may also contribute to inhibiting IRF3 activation and nuclear translocation (65).

In contrast to impaired *Ifn*-α/β mRNA, *Ifit2* deficiency did not alter mRNA expression of either proinflammatory cytokines or chemokines, consistent with similar cellular CNS inflammation. Furthermore, neither *ex vivo*-purified microglia, infiltrating monocytes, nor BMDM cultures showed significantly reduced cytokine or chemokine mRNA or protein expression patterns. These results suggested that Ifit2 specifically regulates the IFN-α/β induction pathway. These results are in contrast to reduced levels of IL-6 and TNF in the absence of Ifit2 in an LPS-induced septic shock model, despite similarly negative effects on IFN-α/β expression (19). The diverging results may be attributable to the distinct signaling molecules, as well as differences in strength of activation in the TLR4 versus MDA5 pathways, and thus highlight the plasticity of Ifit2 interactions.

Although regulation of IFN-α/β expression during viral infections has been reported for human IFITs, this study is the first report to support a protective function of murine Ifit2 in promoting IFN-α/β induction *in vitro* and *in vivo* using the neurotropic coronavirus encephalitis model. While Ifit2-enhanced IRF3 phosphorylation contributes to enhanced IFN-α/β induction, the precise mechanisms by which Ifit2 interacts with components of the MDA5 pathway remain to be elucidated, but they are likely to be MHV specific. This is indicated by the absence of effects of Ifit2 deficiency on the pathogenesis of EMCV (20), although this virus also induces IFN-α/β via MDA5 (66) and does not have 2′-O-methylated 5′-capped mRNAs (15). Minimal effects on proinflammatory cytokine and chemokine mRNA levels, consistent with similar CNS inflammatory infiltrates, further supports a specific interference of Ifit2 in the IFN-α/β induction pathway. The novel role of murine Ifit2 in promoting type I IFN responses is thus reminiscent of IFN-α/β modulation by human IFIT3.

ACKNOWLEDGMENTS

This study was supported by National Institutes of Health grants P01 NS064932 (C.C.B.) and CA068782 (G.C.S.).

We thank Volker Thiel for providing MHV-A59 expressing EGFP and wt MHV-A59 viruses. We thank Mi Widness for breeding mice. We also thank Jennifer Powers for FACS purifications, Wen Wei and Eric Barron for their assistance with the histopathology, Anabelle Visperas for helping with ELISAs, and Tim Phares for editorial help.

REFERENCES

1. **Kumar H, Kawai T, Akira S.** 2009. Pathogen recognition in the innate immune response. Biochem. J. **420:**1–16. http://dx.doi.org/10.1042/BJ20090272.
2. **Wilkins C, Gale M, Jr.** 2010. Recognition of viruses by cytoplasmic sensors. Curr. Opin. Immunol. **22:**41–47. http://dx.doi.org/10.1016/j.coi.2009.12.003.
3. **Samuel CE.** 2001. Antiviral actions of interferons. Clin. Microbiol. Rev. **14:**778–809. http://dx.doi.org/10.1128/CMR.14.4.778-809.2001.
4. **Schoggins JW, Rice CM.** 2011. Interferon-stimulated genes and their antiviral effector functions. Curr. Opin. Virol. **1:**519–525. http://dx.doi.org/10.1016/j.coviro.2011.10.008.
5. **Cho H, Proll SC, Szretter KJ, Katze MG, Gale M, Jr, Diamond MS.** 2013. Differential innate immune response programs in neuronal subtypes determine susceptibility to infection in the brain by positive-stranded RNA viruses. Nat. Med. **19:**458–464. http://dx.doi.org/10.1038/nm.3108.
6. **Zhao L, Birdwell LD, Wu A, Elliott R, Rose KM, Phillips JM, Li Y, Grinspan J, Silverman RH, Weiss SR.** 2013. Cell-type-specific activation

of the oligoadenylate synthetase-RNase L pathway by a murine coronavirus. J. Virol. **87:**8408–8418. http://dx.doi.org/10.1128/JVI.00769-13.
7. **Diamond MS, Farzan M.** 2013. The broad-spectrum antiviral functions of IFIT and IFITM proteins. Nat. Rev. Immunol. **13:**46–57.
8. **Fensterl V, Sen GC.** 2011. The ISG56/IFIT1 gene family. J. Interferon Cytokine Res. **31:**71–78. http://dx.doi.org/10.1089/jir.2010.0101.
9. **Wacher C, Muller M, Hofer MJ, Getts DR, Zabaras R, Ousman SS, Terenzi F, Sen GC, King NJ, Campbell IL.** 2007. Coordinated regulation and widespread cellular expression of interferon-stimulated genes (ISG) ISG-49, ISG-54, and ISG-56 in the central nervous system after infection with distinct viruses. J. Virol. **81:**860–871. http://dx.doi.org/10.1128/JVI.01167-06.
10. **Terenzi F, Pal S, Sen GC.** 2005. Induction and mode of action of the viral stress-inducible murine proteins, P56 and P54. Virology **340:**116–124. http://dx.doi.org/10.1016/j.virol.2005.06.011.
11. **Hui DJ, Bhasker CR, Merrick WC, Sen GC.** 2003. Viral stress-inducible protein p56 inhibits translation by blocking the interaction of eIF3 with the ternary complex eIF2 · GTP · Met-tRNAi. J. Biol. Chem. **278:**39477–39482. http://dx.doi.org/10.1074/jbc.M305038200.
12. **Terenzi F, Hui DJ, Merrick WC, Sen GC.** 2006. Distinct induction patterns and functions of two closely related interferon-inducible human genes, ISG54 and ISG56. J. Biol. Chem. **281:**34064–34071. http://dx.doi.org/10.1074/jbc.M605771200.
13. **Pichlmair A, Lassnig C, Eberle CA, Gorna MW, Baumann CL, Burkard TR, Burckstummer T, Stefanovic A, Krieger S, Bennett KL, Rulicke T, Weber F, Colinge J, Muller M, Superti-Furga G.** 2011. IFIT1 is an antiviral protein that recognizes 5′-triphosphate RNA. Nat. Immunol. **12:**624–630. http://dx.doi.org/10.1038/ni.2048.
14. **Daffis S, Szretter KJ, Schriewer J, Li J, Youn S, Errett J, Lin TY, Schneller S, Zust R, Dong H, Thiel V, Sen GC, Fensterl V, Klimstra WB, Pierson TC, Buller RM, Gale M, Jr, Shi PY, Diamond MS.** 2010. 2′-O methylation of the viral mRNA cap evades host restriction by IFIT family members. Nature **468:**452–456. http://dx.doi.org/10.1038/nature09489.
15. **Zust R, Cervantes-Barragan L, Habjan M, Maier R, Neuman BW, Ziebuhr J, Szretter KJ, Baker SC, Barchet W, Diamond MS, Siddell SG, Ludewig B, Thiel V.** 2011. Ribose 2′-O-methylation provides a molecular signature for the distinction of self and non-self mRNA dependent on the RNA sensor Mda5. Nat. Immunol. **12:**137–143. http://dx.doi.org/10.1038/ni.1979.
16. **Yang Z, Liang H, Zhou Q, Li Y, Chen H, Ye W, Chen D, Fleming J, Shu H, Liu Y.** 2012. Crystal structure of ISG54 reveals a novel RNA binding structure and potential functional mechanisms. Cell Res. **22:**1328–1338. http://dx.doi.org/10.1038/cr.2012.111.
17. **Li Y, Li C, Xue P, Zhong B, Mao AP, Ran Y, Chen H, Wang YY, Yang F, Shu HB.** 2009. ISG56 is a negative-feedback regulator of virus-triggered signaling and cellular antiviral response. Proc. Natl. Acad. Sci. U. S. A. **106:**7945–7950. http://dx.doi.org/10.1073/pnas.0900818106.
18. **Liu XY, Chen W, Wei B, Shan YF, Wang C.** 2011. IFN-induced TPR protein IFIT3 potentiates antiviral signaling by bridging MAVS and TBK1. J. Immunol. **187:**2559–2568. http://dx.doi.org/10.4049/jimmunol.1100963.
19. **Siegfried A, Berchtold S, Manncke B, Deuschle E, Reber J, Ott T, Weber M, Kalinke U, Hofer MJ, Hatesuer B, Schughart K, Gailus-Durner V, Fuchs H, Hrabe de Angelis M, Weber F, Hornef MW, Autenrieth IB, Bohn E.** 2013. IFIT2 is an effector protein of type I IFN-mediated amplification of lipopolysaccharide (LPS)-induced TNF-alpha secretion and LPS-induced endotoxin shock. J. Immunol. **191:**3913–3921. http://dx.doi.org/10.4049/jimmunol.1203305.
20. **Fensterl V, Wetzel JL, Ramachandran S, Ogino T, Stohlman SA, Bergmann CC, Diamond MS, Virgin HW, Sen GC.** 2012. Interferon-induced Ifit2/ISG54 protects mice from lethal VSV neuropathogenesis. PLoS Pathog. **8:**e1002712. http://dx.doi.org/10.1371/journal.ppat.1002712.
21. **Cho H, Shrestha B, Sen GC, Diamond MS.** 2013. A role for ifit2 in restricting West Nile virus infection in the brain. J. Virol. **87:**8363–8371. http://dx.doi.org/10.1128/JVI.01097-13.
22. **Fiette L, Aubert C, Muller U, Huang S, Aguet M, Brahic M, Bureau JF.** 1995. Theiler's virus infection of 129Sv mice that lack the interferon alpha/beta or interferon gamma receptors. J. Exp. Med. **181:**2069–2076. http://dx.doi.org/10.1084/jem.181.6.2069.
23. **Muller U, Steinhoff U, Reis LF, Hemmi S, Pavlovic J, Zinkernagel RM, Aguet M.** 1994. Functional role of type I and type II interferons in antiviral defense. Science **264:**1918–1921. http://dx.doi.org/10.1126/science.8009221.
24. **Ryman KD, Klimstra WB, Nguyen KB, Biron CA, Johnston RE.** 2000. Alpha/beta interferon protects adult mice from fatal Sindbis virus infection and is an important determinant of cell and tissue tropism. J. Virol. **74:**3366–3378. http://dx.doi.org/10.1128/JVI.74.7.3366-3378.2000.
25. **Samuel MA, Diamond MS.** 2005. Alpha/beta interferon protects against lethal West Nile virus infection by restricting cellular tropism and enhancing neuronal survival. J. Virol. **79:**13350–13361. http://dx.doi.org/10.1128/JVI.79.21.13350-13361.2005.
26. **Cervantes-Barragan L, Zust R, Weber F, Spiegel M, Lang KS, Akira S, Thiel V, Ludewig B.** 2007. Control of coronavirus infection through plasmacytoid dendritic-cell-derived type I interferon. Blood **109:**1131–1137.
27. **Ireland DD, Stohlman SA, Hinton DR, Atkinson R, Bergmann CC.** 2008. Type I interferons are essential in controlling neurotropic coronavirus infection irrespective of functional CD8 T cells. J. Virol. **82:**300–310. http://dx.doi.org/10.1128/JVI.01794-07.
28. **Ireland DD, Stohlman SA, Hinton DR, Kapil P, Silverman RH, Atkinson RA, Bergmann CC.** 2009. RNase L mediated protection from virus induced demyelination. PLoS Pathog. **5:**e1000602. http://dx.doi.org/10.1371/journal.ppat.1000602.
29. **Szretter KJ, Daniels BP, Cho H, Gainey MD, Yokoyama WM, Gale M, Jr, Virgin HW, Klein RS, Sen GC, Diamond MS.** 2012. 2′-O methylation of the viral mRNA cap by West Nile virus evades ifit1-dependent and -independent mechanisms of host restriction in vivo. PLoS Pathog. **8:**e1002698. http://dx.doi.org/10.1371/journal.ppat.1002698.
30. **Zhao L, Jha BK, Wu A, Elliott R, Ziebuhr J, Gorbalenya AE, Silverman RH, Weiss SR.** 2012. Antagonism of the interferon-induced OAS-RNase L pathway by murine coronavirus ns2 protein is required for virus replication and liver pathology. Cell Host Microbe **11:**607–616. http://dx.doi.org/10.1016/j.chom.2012.04.011.
31. **Kristiansen H, Gad HH, Eskildsen-Larsen S, Despres P, Hartmann R.** 2011. The oligoadenylate synthetase family: an ancient protein family with multiple antiviral activities. J. Interferon Cytokine Res. **31:**41–47. http://dx.doi.org/10.1089/jir.2010.0107.
32. **Eriksson KK, Cervantes-Barragan L, Ludewig B, Thiel V.** 2008. Mouse hepatitis virus liver pathology is dependent on ADP-ribose-1″-phosphatase, a viral function conserved in the alpha-like supergroup. J. Virol. **82:**12325–12334. http://dx.doi.org/10.1128/JVI.02082-08.
33. **Rempel JD, Murray SJ, Meisner J, Buchmeier MJ.** 2004. Differential regulation of innate and adaptive immune responses in viral encephalitis. Virology **318:**381–392. http://dx.doi.org/10.1016/j.virol.2003.09.023.
34. **Savarin C, Stohlman SA, Rietsch AM, Butchi N, Ransohoff RM, Bergmann CC.** 2011. MMP9 deficiency does not decrease blood-brain barrier disruption, but increases astrocyte MMP3 expression during viral encephalomyelitis. Glia **59:**1770–1781. http://dx.doi.org/10.1002/glia.21222.
35. **Fleming JO, Trousdale MD, el-Zaatari FA, Stohlman SA, Weiner LP.** 1986. Pathogenicity of antigenic variants of murine coronavirus JHM selected with monoclonal antibodies. J. Virol. **58:**869–875.
36. **Kapil P, Butchi NB, Stohlman SA, Bergmann CC.** 2012. Oligodendroglia are limited in type I interferon induction and responsiveness in vivo. Glia **60:**1555–1566. http://dx.doi.org/10.1002/glia.22375.
37. **Gonzalez JM, Bergmann CC, Fuss B, Hinton DR, Kangas C, Macklin WB, Stohlman SA.** 2005. Expression of a dominant negative IFN-gammareceptor on mouse oligodendrocytes. Glia **51:**22–34. http://dx.doi.org/10.1002/glia.20182.
38. **Phares TW, Marques CP, Stohlman SA, Hinton DR, Bergmann CC.** 2011. Factors supporting intrathecal humoral responses following viral encephalomyelitis. J. Virol. **85:**2589–2598. http://dx.doi.org/10.1128/JVI.02260-10.
39. **Bergmann CC, Parra B, Hinton DR, Chandran R, Morrison M, Stohlman SA.** 2003. Perforin-mediated effector function within the central nervous system requires IFN-gamma-mediated MHC up-regulation. J. Immunol. **170:**3204–3213.
40. **Phares TW, Ramakrishna C, Parra GI, Epstein A, Chen L, Atkinson R, Stohlman SA, Bergmann CC.** 2009. Target-dependent B7-H1 regulation contributes to clearance of central nervous system infection and dampens morbidity. J. Immunol. **182:**5430–5438. http://dx.doi.org/10.4049/jimmunol.0803557.
41. **Uze G, Di Marco S, Mouchel-Vielh E, Monneron D, Bandu MT, Horisberger MA, Dorques A, Lutfalla G, Mogensen KE.** 1994. Domains of interaction between alpha interferon and its receptor components. J. Mol. Biol. **243:**245–257. http://dx.doi.org/10.1006/jmbi.1994.1651.
42. **Terenzi F, White C, Pal S, Williams BR, Sen GC.** 2007. Tissue-specific and inducer-specific differential induction of ISG56 and ISG54 in mice. J. Virol. **81:**8656–8665. http://dx.doi.org/10.1128/JVI.00322-07.

43. **Reiss CS, Plakhov IV, Komatsu T.** 1998. Viral replication in olfactory receptor neurons and entry into the olfactory bulb and brain. Ann. N. Y. Acad. Sci. **855:**751–761. http://dx.doi.org/10.1111/j.1749-6632.1998.tb10655.x.
44. **van den Pol AN.** 2006. Viral infections in the developing and mature brain. Trends Neurosci. **29:**398–406. http://dx.doi.org/10.1016/j.tins.2006.06.002.
45. **van den Pol AN, Dalton KP, Rose JK.** 2002. Relative neurotropism of a recombinant rhabdovirus expressing a green fluorescent envelope glycoprotein. J. Virol. **76:**1309–1327. http://dx.doi.org/10.1128/JVI.76.3.1309-1327.2002.
46. **Vernon PS, Griffin DE.** 2005. Characterization of an in vitro model of alphavirus infection of immature and mature neurons. J. Virol. **79:**3438–3447. http://dx.doi.org/10.1128/JVI.79.6.3438-3447.2005.
47. **Lavi E, Gilden DH, Highkin MK, Weiss SR.** 1984. Persistence of mouse hepatitis virus A59 RNA in a slow virus demyelinating infection in mice as detected by in situ hybridization. J. Virol. **51:**563–566.
48. **Miura TA, Travanty EA, Oko L, Bielefeldt-Ohmann H, Weiss SR, Beauchemin N, Holmes KV.** 2008. The spike glycoprotein of murine coronavirus MHV-JHM mediates receptor-independent infection and spread in the central nervous systems of Ceacam1a−/− mice. J. Virol. **82:**755–763. http://dx.doi.org/10.1128/JVI.01851-07.
49. **Phillips JJ, Chua MM, Lavi E, Weiss SR.** 1999. Pathogenesis of chimeric MHV4/MHV-A59 recombinant viruses: the murine coronavirus spike protein is a major determinant of neurovirulence. J. Virol. **73:**7752–7760.
50. **Roth-Cross JK, Bender SJ, Weiss SR.** 2008. Murine coronavirus mouse hepatitis virus is recognized by MDA5 and induces type I interferon in brain macrophages/microglia. J. Virol. **82:**9829–9838. http://dx.doi.org/10.1128/JVI.01199-08.
51. **Cervantes-Barragan L, Kalinke U, Zust R, Konig M, Reizis B, Lopez-Macias C, Thiel V, Ludewig B.** 2009. Type I IFN-mediated protection of macrophages and dendritic cells secures control of murine coronavirus infection. J. Immunol. **182:**1099–1106.
52. **Gonzalez JM, Bergmann CC, Ramakrishna C, Hinton DR, Atkinson R, Hoskin J, Macklin WB, Stohlman SA.** 2006. Inhibition of interferon-gamma signaling in oligodendroglia delays coronavirus clearance without altering demyelination. Am. J. Pathol. **168:**796–804. http://dx.doi.org/10.2353/ajpath.2006.050496.
53. **Hindinger C, Bergmann CC, Hinton DR, Phares TW, Parra GI, Hussain S, Savarin C, Atkinson RD, Stohlman SA.** 2012. IFN-gamma signaling to astrocytes protects from autoimmune mediated neurological disability. PLoS One **7:**e42088. http://dx.doi.org/10.1371/journal.pone.0042088.
54. **Hua LL, Kim MO, Brosnan CF, Lee SC.** 2002. Modulation of astrocyte inducible nitric oxide synthase and cytokine expression by interferon beta is associated with induction and inhibition of interferon gamma-activated sequence binding activity. J. Neurochem. **83:**1120–1128. http://dx.doi.org/10.1046/j.1471-4159.2002.01226.x.
55. **Okada K, Kuroda E, Yoshida Y, Yamashita U, Suzumura A, Tsuji S.** 2005. Effects of interferon-beta on the cytokine production of astrocytes. J. Neuroimmunol. **159:**48–54. http://dx.doi.org/10.1016/j.jneuroim.2004.09.013.
56. **Savarin C, Stohlman SA, Atkinson R, Ransohoff RM, Bergmann CC.** 2010. Monocytes regulate T cell migration through the glia limitans during acute viral encephalitis. J. Virol. **84:**4878–4888. http://dx.doi.org/10.1128/JVI.00051-10.
57. **Servant MJ, Grandvaux N, tenOever BR, Duguay D, Lin R, Hiscott J.** 2003. Identification of the minimal phosphoacceptor site required for in vivo activation of interferon regulatory factor 3 in response to virus and double-stranded RNA. J. Biol. Chem. **278:**9441–9447. http://dx.doi.org/10.1074/jbc.M209851200.
58. **Flodstrom-Tullberg M, Hultcrantz M, Stotland A, Maday A, Tsai D, Fine C, Williams B, Silverman R, Sarvetnick N.** 2005. RNase L and double-stranded RNA-dependent protein kinase exert complementary roles in islet cell defense during coxsackievirus infection. J. Immunol. **174:**1171–1177.
59. **Samuel MA, Whitby K, Keller BC, Marri A, Barchet W, Williams BR, Silverman RH, Gale M, Jr, Diamond MS.** 2006. PKR and RNase L contribute to protection against lethal West Nile Virus infection by controlling early viral spread in the periphery and replication in neurons. J. Virol. **80:**7009–7019. http://dx.doi.org/10.1128/JVI.00489-06.
60. **Zhou A, Paranjape J, Brown TL, Nie H, Naik S, Dong B, Chang A, Trapp B, Fairchild R, Colmenares C, Silverman RH.** 1997. Interferon action and apoptosis are defective in mice devoid of 2′,5′-oligoadenylate-dependent RNase L. EMBO J. **16:**6355–6363. http://dx.doi.org/10.1093/emboj/16.21.6355.
61. **Loo YM, Gale M, Jr.** 2011. Immune signaling by RIG-I-like receptors. Immunity **34:**680–692. http://dx.doi.org/10.1016/j.immuni.2011.05.003.
62. **Lu LL, Puri M, Horvath CM, Sen GC.** 2008. Select paramyxoviral V proteins inhibit IRF3 activation by acting as alternative substrates for inhibitor of kappaB kinase epsilon (IKKe)/TBK1. J. Biol. Chem. **283:**14269–14276. http://dx.doi.org/10.1074/jbc.M710089200.
63. **White TC, Yi Z, Hogue BG.** 2007. Identification of mouse hepatitis coronavirus A59 nucleocapsid protein phosphorylation sites. Virus Res. **126:**139–148. http://dx.doi.org/10.1016/j.virusres.2007.02.008.
64. **Wilbur SM, Nelson GW, Lai MM, McMillan M, Stohlman SA.** 1986. Phosphorylation of the mouse hepatitis virus nucleocapsid protein. Biochem. Biophys. Res. Commun. **141:**7–12. http://dx.doi.org/10.1016/S0006-291X(86)80326-6.
65. **Wang G, Chen G, Zheng D, Cheng G, Tang H.** 2011. PLP2 of mouse hepatitis virus A59 (MHV-A59) targets TBK1 to negatively regulate cellular type I interferon signaling pathway. PLoS One **6:**e17192. http://dx.doi.org/10.1371/journal.pone.0017192.
66. **Gitlin L, Barchet W, Gilfillan S, Cella M, Beutler B, Flavell RA, Diamond MS, Colonna M.** 2006. Essential role of mda-5 in type I IFN responses to polyriboinosinic:polyribocytidylic acid and encephalomyocarditis picornavirus. Proc. Natl. Acad. Sci. U. S. A. **103:**8459–8464. http://dx.doi.org/10.1073/pnas.0603082103.